# Simulation-Based Investigation of Curtain Gas Effect on Metal-Organic Chemical Vapor Deposition Growth of Two-Dimensional Transition Metal Dichalcogenides

*Feng Zhang,*[1,2] *Fanyu Zeng,*[1,2] *Daichi Kozawa,*[1] *and Ryo Kitaura*[*, 1]

[1] Research Center for Materials Nanoarchitectonics, National Institute for Materials Science, 1-1 Namiki, Tsukuba 305-0044, Japan

[2] Department of Chemistry, Nagoya University, Nagoya 464-8601, Japan

Abstract

This study examines the impact of curtain gas flow on Metal-Organic Chemical Vapor Deposition (MOCVD) growth of two-dimensional (2D) transition metal dichalcogenides using Finite Element Method simulations and growth experiments. The simulation results demonstrate that the curtain gas changes precursor transfer dynamics, concentrates the flow towards the substrate, and potentially lowers contamination from chamber walls. The simulation findings are supported by experimental validation using tungsten and sulfur sources, which confirms that curtain gas flow is critical in enhancing the reproducibility of 2D $WS_2$ growth. The research highlights the need to optimize gas flow dynamics in MOCVD processes to unlock the full potential of 2D materials in future electronic devices.

## Introduction

Two-dimensional (2D) materials have been of great interest due to their unique properties, which can lead to the next-generation electronic devices[1-3]. For example, 2D transition metal dichalcogenides (TMDs) can have a bandgap typically ranging from 1-2 eV, making them potential candidates for transistors to overcome the adverse short-channel effects[4]. In fact, ultrashort channel devices with gate lengths of 1 nm have been demonstrated using TMDs-based transistors with carbon nanotubes as ultrathin backgate electrodes[5]. The high performance of these ultrashort devices, subthreshold swings of ~ 65 mV and on/off ratios of ~ $10^6$ even at 1-nm gate length, is primarily due to the ultrathin structure of the 2D TMDs[6]. Also, carriers in TMDs can have extra degrees of freedom that come from the momentum space, known as the Valley Degrees of Freedom (VDOF)[7]. The VDOF can be generated and detected optically, which may lead to future quantum devices based on VDOF manipulation. In addition, fabricating vertical or horizontal heterostructures can provide a way to manipulate the electronic band structure and spatial symmetry in 2D materials[8, 9]. This allows for more flexibility in band engineering, which can expand the potential applications for these materials.

Previous studies have shown that chemical vapor deposition (CVD) is a viable method for synthesizing 2D TMDs, making it a potential way for wafer-scale growth for device applications[10-12]. Most previous studies on CVD growth have utilized solid sources like metal oxides and chlorides. These metal sources can be vaporized at high temperatures and react with chalcogen sources, typically elemental chalcogen, to form 2D TMDs crystals with lateral sizes much larger than those obtained by the mechanical exfoliation method. However, these source supplies are typically not very stable because the source supply relies on sublimation. On the other hand, Metal-

Organic CVD (MOCVD), where volatile sources are delivered as vapors, can provide a more stable source supply, allowing more precise control for future device applications[13-15].

In a typical MOCVD process, a silicon or sapphire substrate is placed in a quartz tube reactor. Metal-organic and sulfur sources are fed through the tube and decomposed to create active species, ultimately forming 2D materials on the substrate. During this process, decomposed sources attach to the quart-tube surface, which can lead to contamination in the following growth processes. The typical way to avoid contamination is to use a cold-wall chamber to prevent the vaporization of the precursor from the chamber walls. Also, adding a curtain gas flow surrounding the source flow is expected to reduce contamination further[16, 17]. However, the underlying mechanisms and subsequent effects of the curtain flow in MOCVD growth of 2D TMDs are not fully understood.

In this study, we performed finite element method (FEM) simulation to investigate the curtain gas effect. We first built a model of our MOCVD equipment to perform FEM simulation and extracted field information, including temperature, fluid, and molar flux. The simulation showed that the curtain gas flow changes the precursor transfer from the showerhead to the substrate; the precursor flow is more focused on the substrate by the curtain flow. To verify the simulation results and to gain a deeper insight into the influence of the curtain gas, corresponding experiments were carried out with Bis(t-butylimido)bis(dimethylamino)tungsten and diethyl sulfide as W and S sources, respectively. In the case of growth without curtain flow, we observed that the order of each experiment had a significant effect on the growth results, even under the same growth conditions. This order dependence may result from the contamination originating from the chamber wall, indicating the importance of curtain flow in the MOCVD growth of 2D materials. Our findings have revealed an influential factor in the CVD growth of 2D materials, potentially leading to an improved chamber design for future 2D-materials-based devices.

## Experimental Section

**Finite Element Simulation.** The finite element simulation was performed using COMSOL Multiphysics software. We built a model of the MOCVD chamber based on the actual chamber used in the growth experiments with mesh sizes ranging from 0.8 to 20 mm depending on the locations; we used fine mesh around the center region where the showerhead and susceptor are placed, while coarse mesh was used at locations far from the center region. The simulation included the heat transfer, fluid flow, and mass transfer modules. Stationary simulation was used in this work to approximate the actual growth process. The reactions were not included in the simulation because we focused on the curtain gas effect, which is expected to be insensitive to reaction details. More details were discussed in supporting information.

**Synthesis of $WS_2$.** MOCVD growth of $WS_2$ on $SiO_2$/Si substrate was performed using a home-built MOCVD system. Metal and sulfur sources, bis(t-butylimido)bis(dimethylamino)tungsten and diethyl sulfide, were purchased from Gas-Phase Growth Ltd. and used as received. Precursor temperatures were kept constant throughout the growth processes to maintain vapor pressures constant; precursors stored in stainless steel bottles were placed in constant-temperature water baths. The precursor vapor was transported by Ar bubbling with flow rates of 30 and 20 sccm for the W and S sources, respectively. In some cases, an Ar curtain flow with a flow rate of 100 sccm was also added. The growth was performed for 15 min under 10 kPa at 750 ℃. The entire growth process, including heater control, flow rate control, and valve operation, was performed automatically using LabVIEW-based software.

**Sample Characterization.** Raman and photoluminescence (PL) spectra were measured using a home-built microspectroscopy system equipped with a spectrometer (Teledyne Princeton Ins. IsoPlane SCT320). A CW excitation laser with a wavelength of 532 nm was focused on a sample

with a × 100 objective (N.A. 0.8), and the PL signals were detected with a charge-coupled device (Teledyne Princeton Ins. PIXIS 1024BReXcelon). The PL images were measured with a home-built optical microscope equipped with a back-illuminated sCMOS camera (KURO, Teledyne Princeton Ins.). Five positions of each sample were measured with a ×10 objective (N.A. 0.3), and the average PL intensity, nucleation density, and average size were extracted from the obtained PL images using ImageJ software[18]. All measurements were performed at room temperature under ambient conditions.

**Partial Pressure Measurement.** The partial pressure inside the growth chamber was measured by a mass spectrometer (BMG2-201, ULVAC, Inc.) equipped with an MOCVD chamber (Schematic see Fig. S4(a)). During the growth process, the gas was introduced from the chamber to the mass spectrometer through a variable leak valve. We utilize a turbomolecular pump for differential pumping to maintain a suitable working pressure (less than $10^{-3}$ Pa) for the spectrometer.

**Results and Discussion**

Figure 1a shows a schematic of the precursor supply system, where the precursor vapors are mixed before passing through the showerhead and flowing onto the substrate. Figure 1b shows the precursor supply with additional Ar flow surrounding the precursor flow as a gas curtain. To investigate the difference between these cases (with- and without-curtain cases), we built a numerical model of our MOCVD chamber to investigate the flow inside the chamber in detail. Figure 1c shows the Ar flow velocity distribution in the with-curtain case, where the arrows represent the flow direction near the substrate. The arrows in Fig. 1c demonstrate that the flow condition creates a uniform fluid field, facilitating the uniform growth of $WS_2$[19, 20]. The S source

concentration distribution on the substrate surface is shown in Fig 1d. The normalized concentration image shows excellent uniformity, with a 2% difference at the corners, which is unavoidable due to the edge effect[21]. This uniform concentration distribution is not achievable in conventional powder-source CVD with a tubular-type reactor because the gradual change in concentration along the tube axis inevitably exists[22]. We found that the velocity and concentration distributions in the without-curtain case are almost identical to the with-curtain case (Fig. S1); this result demonstrates that the curtain flow does not interrupt the precursor supply.

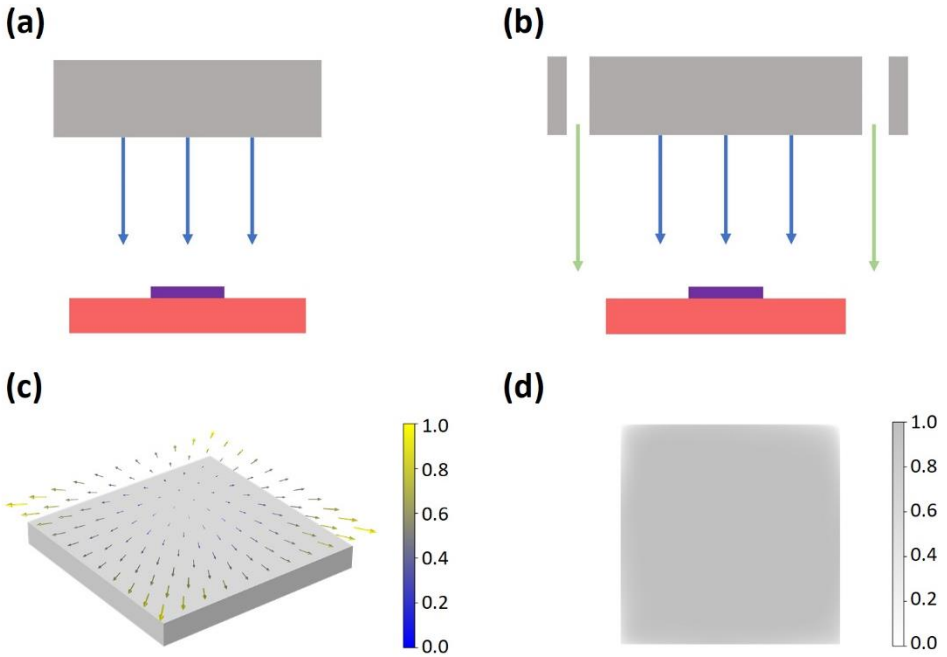


**Figure 1.** The strategy of the mental-organic source supply in the MOCVD process and simulated results on and near the substrate. Schematic illustration of the mental-organic supply part of without (a) and with (b) curtain Argon cases, from showerhead to substrate on the heater. (c) Normalized velocity distribution arrow near the substrate surface. (d) Normalized concentration distribution on the substrate surface.

The in-chamber sulfur source concentration was investigated to see the mass transfer mode in without- and with-curtain cases. Figures 2a and b show the concentration distributions of the without- and with-curtain cases, respectively. Note that the difference in simulation conditions between without- and with-curtain cases is only the absence or presence of the curtain flow. We

fixed all other conditions, including sulfur and metal precursor flow rates, to investigate the pure effect of adding curtain flow. The concentration profiles along the dashed line A-A' are plotted in Fig. 2c, showing that the with-curtain case shows an S concentration higher than the without-curtain case in the entire region from the substrate surface to the showerhead. The concentration line profile along the B-B' also presented to clearly show the difference in two cases (raw data see Fig. S3). The 1.7% concentration difference on the substrate surface (the inset in Fig. 2c) is attributed to variations in the total flow rate, with a higher flow rate in the with-curtain case facilitating the precursor supply on the substrate surface. Figure 2d shows the molar flux along the dashed line in Fig. 2b, indicating a maximum difference of 43.1% between the two cases. This difference means more S precursors are transferred along the dashed line under the same amount of S precursor supply. The results shown here indicate that curtain flow improves the concentration and velocity of the S source by concentrating the precursor supply flow in the center of the chamber.

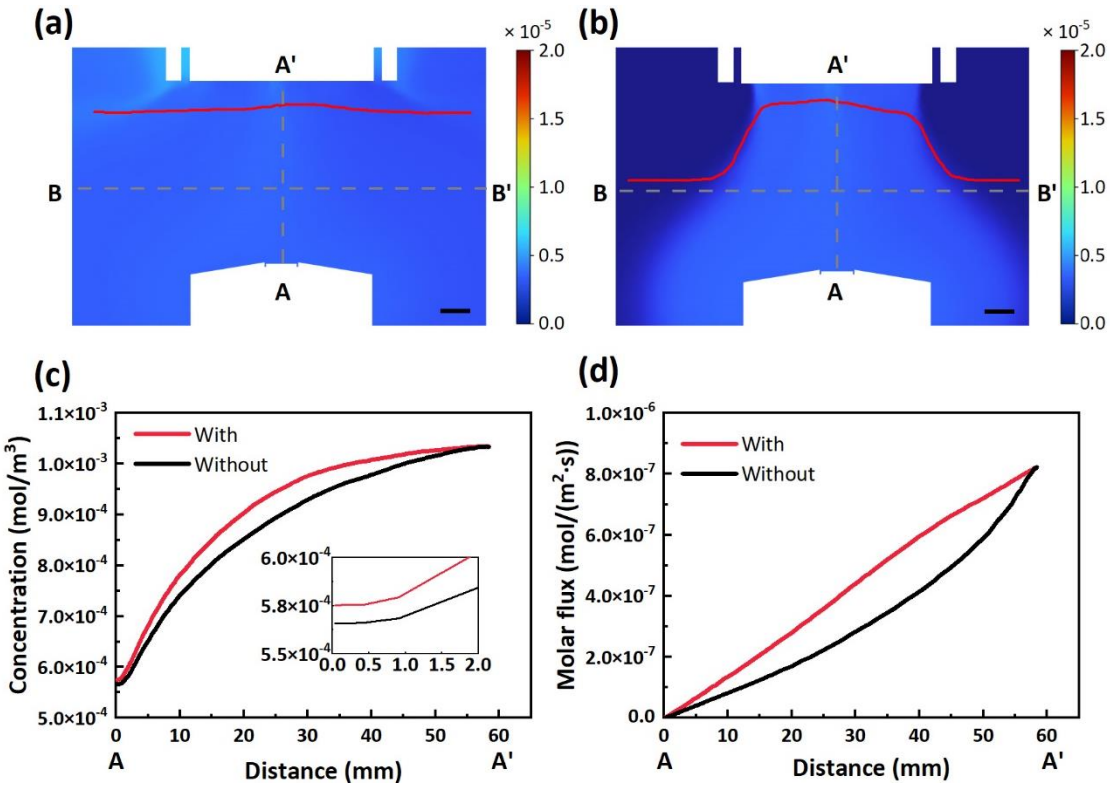


**Figure 2.** Simulated field profile of with- and without-curtain cases. Two-dimensional map showing the sulfur source distribution in the without (a) and with (b) curtain case. The red curves in (a) and (b) represent the concentration distribution along the B-B' dashed lines. (c) Sulfur concentration profile along the A-A' dashed line, from the substrate surface to the bottom of the showerhead. (d) Calculated molar flux along the A-A' dashed line. Scale bar = 10 mm.

To verify the curtain-flow effect on MOCVD processes, we synthesized $WS_2$ under a series of growth conditions and performed characterization with optical microscopy and Raman and photoluminescence (PL) spectroscopy. Figures 3a, b, and c show a typical optical image, Raman, and PL spectrum, respectively. As seen in Fig. 3a, all $WS_2$ flakes are triangular with a lateral size of typically several tens of micrometers. The triangular shape is consistent with previously reported CVD-grown $WS_2$, where zigzag edges preferentially appear during growth processes[23]. As seen in the Raman spectrum, there are two prominent peaks at ~350 and ~420 $cm^{-1}$, which correspond to $E^1_{2g}$ and $A_{1g}$ vibrational modes of $WS_2$, respectively. Note that the additional Raman peak around 520 $cm^{-1}$ arises from the vibrational mode of a Si substrate. The PL spectrum exhibits

a sharp peak at 1.96 eV with a full width at half maximum value of approximately 50 meV (Fig. 3c.), consistent with previous results on MOCVD synthesized $WS_2$[24]. The detailed comparison of the Raman and PL spectrum of each of our samples is shown in Fig. S2.

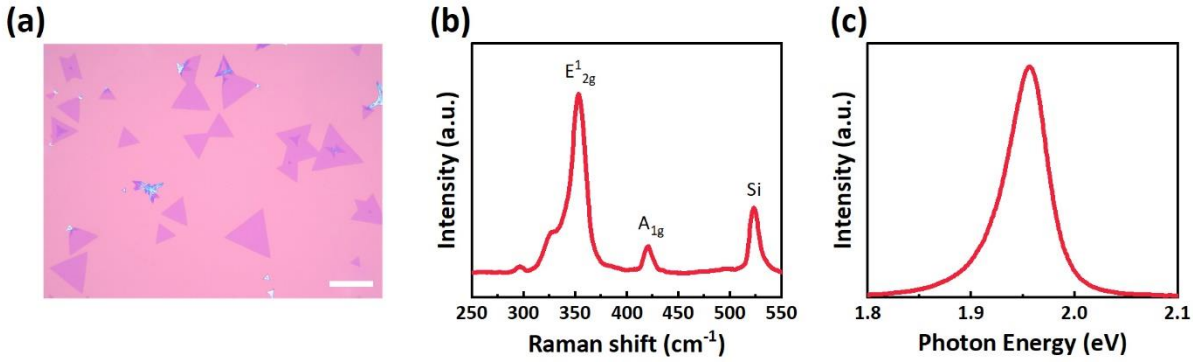


**Figure 3.** Characterization of synthesized typical crystals. (a) Optical microscope image of growth monolayer $WS_2$ sample. (b) Raman spectra of the obtained $WS_2$. (c) Photoluminescence spectra of the $WS_2$. Scale bar = 100 μm.

**Table 1.** Statistics of the nucleation density, crystal size, and mean PL intensity

| Sample | Nucleation density ($mm^{-2}$) | Average crystal size (μm) | Mean PL intensity |
|---|---|---|---|
| **With-1** | 58.5 ± 11.7 | 9.4 ± 6.7 | 156.6 ± 34.1 |
| **With-2** | 60.7 ± 18.7 | 11.2 ± 3.8 | 158.8 ± 45.1 |
| **With-3** | 58.5 ± 7.1 | 9.4 ± 3.8 | 153.2 ± 35.8 |
| **Without-1** | 25.7 ± 14.0 | 10.6 ± 2.9 | 168.5 ± 75.1 |
| **Without-2** | 51.5± 9.4 | 8.4 ± 7.4 | 150.8 ± 49.8 |
| **Without-3** | 131.1 ± 16.4 | 5.1 ± 3.2 | 135.6 ± 44.1 |

To better understand the differences in CVD growth with- and without-curtain cases, we have performed analyses based on PL imaging, which provides information regarding the quality and size of grown $WS_2$ crystals[25]. Nucleation density, average crystal size, and mean PL intensity

extracted from PL imaging are summarized in Table 1; we have conducted three continuous experiments for with- and without-curtain cases under the same growth conditions. While similar PL intensities are observed for all the with-curtain cases (Fig. 4 a-c), a gradual decrease in PL intensity is seen in the without-curtain cases (Fig. 4 d-f). The crack-like lines correspond to ribbon-like top layers of $WS_2$ grown on top of the bottom layers of $WS_2$; bilayer parts give weak PL intensities because bilayers are indirect semiconductors. Note that the nucleation density in the with-curtain case (Fig 4. a-c) is slightly higher than the without-curtain case (Fig. 4d). As seen in Table 1, in the without-curtain case, the nucleation density increases as the experiment is repeated. Specifically, there is about a 3-fold difference between the $1^{st}$ and $3^{rd}$ experiments, and a corresponding reduction in crystal size is also seen. Also, the mean PL intensity exhibits a significant 24% decrease in the without-curtain case, which suggests poor reproducibility. In contrast, nucleation density, crystal size, and PL intensity do not significantly change in the with-curtain case; 3.7%, 19.5%, and 3.6% differences in nucleation density, crystal size, and PL intensity, respectively.

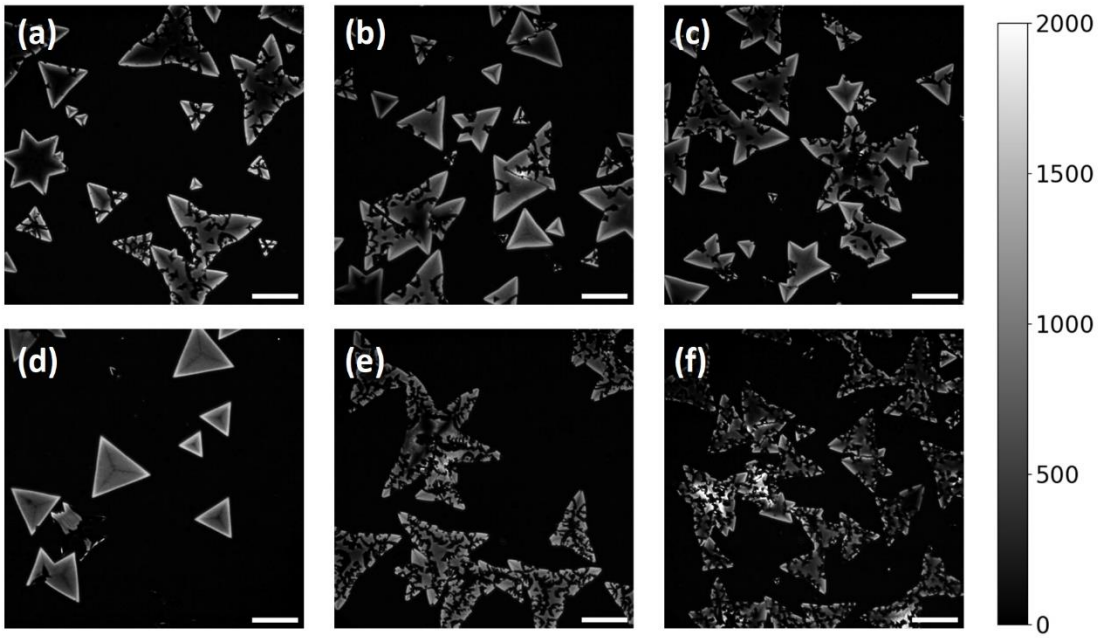

**Figure 4.** PL images of a set of with/without curtain Argon samples. PL images of continuously conducted experiments under the same with (a-c) and without (d-f) curtain Argon condition. Scale bar = 100 μm.

The simulation results demonstrate that the presence of curtain gas leads to more focused fluid flow around the substrate, resulting in an efficient source supply. This efficient supply probably caused larger nucleation density in the initial experiment (Fig. 4a). Additionally, the experimental results suggest that reproducibility is significantly enhanced in the with-curtain case. This consistent trend highlights the critical role of the curtain flow in controlling growth processes. The gradual change of nucleation density and PL intensity indicates that the precursor supply is more susceptible to external influence in the absence of a curtain flow. Based on the simulation results (Fig. 2a, b), we suspect that the less controlled growth is due to the sources remaining in the chamber[26]. The existence of residual sources can be seen in sulfur concentration monitored with a mass spectrometer; sulfur concentration in the chamber increases as experiments are repeated, probably originating from the desorption of sources remaining on the chamber wall. The remaining source can contribute to the growth process in the absence of a curtain flow, leading to promoting nucleation and subsequent crystal growth. In contrast, when a curtain flow is present, the remaining sources are blocked by the curtain flow, thereby providing reproducible growth in all experiments. Details of source concentration evolution during growth processes and the corresponding discussion are given in supporting information (Figs. S4).

## Conclusion

In this work, a simulation-based investigation was conducted to reveal the curtain gas effect on the MOCVD growth process. The curtain gas flow focuses the precursor supply to the central region, resulting in efficient mass transfer to the substrate surface. The corresponding experiments

revealed the effect of the curtain gas flow. Specifically, in the absence of the curtain gas flow, the nucleation density changes depending on the order of the experiments, probably due to the accumulation of the sulfur source in the chamber. The results presented demonstrate that the implementation of curtain flow improves the reproducibility of MOCVD growth by creating a concentrated fluid flow around the substrate, potentially leading to improved chamber design for future 2D-materials-based devices. This simulation-based approach provides a way to visualize physical quantities that are difficult to measure experimentally, providing a clue to understanding and improving complex growth processes.

## Supporting Information

The supporting information is available free of charge at https://pubs.acs.org/doi/*****.

- Concentration and velocity distribution, Raman and PL spectra, concentration profile across the chamber, time dependence of sulfur concentrations, simulation details


## Acknowledgments

R.K. was supported by JSPS KAKENHI Grant No. JP24H02218, JP23H05469, JP22H05458, JP21K18930 and JP20H05664, and JST CREST Grant No. JPMJCR16F3, SCICORP Grant No. JPMJSC2110 and PRESTO Grant No. JPMJPR20A2.

**References**


(1) Liu, C.; Chen, H.; Wang, S.; Liu, Q.; Jiang, Y.-G.; Zhang, D. W.; Liu, M.; Zhou, P., Two-dimensional materials for next-generation computing technologies. *Nature Nanotechnology* **2020,** *15* (7), 545-557

(2) Cheng, Z.; Cao, R.; Wei, K.; Yao, Y.; Liu, X.; Kang, J.; Dong, J.; Shi, Z.; Zhang, H.; Zhang, X., 2D materials enabled next‐generation integrated optoelectronics: from fabrication to applications. *Advanced Science* **2021,** *8* (11), 2003834

(3) Fiori, G.; Bonaccorso, F.; Iannaccone, G.; Palacios, T.; Neumaier, D.; Seabaugh, A.; Banerjee, S. K.; Colombo, L., Electronics based on two-dimensional materials. *Nature nanotechnology* **2014,** *9* (10), 768-779

(4) Jing, X.; Illarionov, Y.; Yalon, E.; Zhou, P.; Grasser, T.; Shi, Y.; Lanza, M., Engineering field effect transistors with 2D semiconducting channels: status and prospects. *Advanced Functional Materials* **2020,** *30* (18), 1901971

(5) Desai, S. B.; Madhvapathy, S. R.; Sachid, A. B.; Llinas, J. P.; Wang, Q.; Ahn, G. H.; Pitner, G.; Kim, M. J.; Bokor, J.; Hu, C., MoS2 transistors with 1-nanometer gate lengths. *Science* **2016,** *354* (6308), 99-102

(6) Zhu, W.; Low, T.; Wang, H.; Ye, P.; Duan, X., Nanoscale electronic devices based on transition metal dichalcogenides. *2D Materials* **2019,** *6* (3), 032004

(7) Mak, K. F.; Xiao, D.; Shan, J., Light–valley interactions in 2D semiconductors. *Nature Photonics* **2018,** *12* (8), 451-460

(8) Liu, Y.; Weiss, N. O.; Duan, X.; Cheng, H.-C.; Huang, Y.; Duan, X., Van der Waals heterostructures and devices. *Nature Reviews Materials* **2016,** *1* (9), 1-17

(9) Calman, E.; Fogler, M.; Butov, L.; Hu, S.; Mishchenko, A.; Geim, A., Indirect excitons in van der Waals heterostructures at room temperature. *Nature communications* **2018,** *9* (1), 1895

(10) Zhou, J.; Lin, J.; Huang, X.; Zhou, Y.; Chen, Y.; Xia, J.; Wang, H.; Xie, Y.; Yu, H.; Lei, J., A library of atomically thin metal chalcogenides. *Nature* **2018,** *556* (7701), 355-359

(11) Chhowalla, M.; Liu, Z.; Zhang, H., Two-dimensional transition metal dichalcogenide (TMD) nanosheets. *Chemical Society Reviews* **2015,** *44* (9), 2584-2586

(12) Xia, J.; Huang, X.; Liu, L.-Z.; Wang, M.; Wang, L.; Huang, B.; Zhu, D.-D.; Li, J.-J.; Gu, C.-Z.; Meng, X.-M., CVD synthesis of large-area, highly crystalline MoSe 2 atomic layers on diverse substrates and application to photodetectors. *Nanoscale* **2014,** *6* (15), 8949-8955

(13) Cwik, S.; Mitoraj, D.; Mendoza Reyes, O.; Rogalla, D.; Peeters, D.; Kim, J.; Schütz, H. M.; Bock, C.; Beranek, R.; Devi, A., Direct growth of MoS2 and WS2 layers by metal organic chemical vapor deposition. *Advanced Materials Interfaces* **2018,** *5* (16), 1800140

(14) Choi, J. H.; Ha, M. J.; Park, J. C.; Park, T. J.; Kim, W. H.; Lee, M. J.; Ahn, J. H., A Strategy for Wafer‐Scale Crystalline MoS2 Thin Films with Controlled Morphology Using Pulsed Metal‐Organic Chemical Vapor Deposition at Low Temperature. *Advanced Materials Interfaces* **2022,** *9* (4), 2101785

(15) Seol, M.; Lee, M. H.; Kim, H.; Shin, K. W.; Cho, Y.; Jeon, I.; Jeong, M.; Lee, H. I.; Park, J.; Shin, H. J., High‐throughput growth of wafer‐scale monolayer transition metal dichalcogenide via vertical ostwald ripening. *Advanced Materials* **2020,** *32* (42), 2003542

(16) Lee, W.; Jeong, M.-C.; Myoung, J.-M., Catalyst-free growth of ZnO nanowires by metal-organic chemical vapour deposition (MOCVD) and thermal evaporation. *Acta Materialia* **2004,** *52* (13), 3949-3957

(17) Lee, W.; Jeong, M.-C.; Myoung, J.-M., Fabrication and application potential of ZnO nanowires grown on GaAs (002) substrates by metal–organic chemical vapour deposition. *Nanotechnology* **2003,** *15* (3), 254
(18) Gustafsson, N.; Culley, S.; Ashdown, G.; Owen, D. M.; Pereira, P. M.; Henriques, R., Fast live-cell conventional fluorophore nanoscopy with ImageJ through super-resolution radial fluctuations. *Nature communications* **2016,** *7* (1), 12471
(19) Momeni, K.; Ji, Y.; Nayir, N.; Sakib, N.; Zhu, H.; Paul, S.; Choudhury, T. H.; Neshani, S.; Van Duin, A. C.; Redwing, J. M., A computational framework for guiding the MOCVD-growth of wafer-scale 2D materials. *npj Computational Materials* **2022,** *8* (1), 240
(20) Hong, W.; Park, C.; Shim, G. W.; Yang, S. Y.; Choi, S.-Y., Wafer-scale uniform growth of an atomically thin MoS2 film with controlled layer numbers by metal–organic chemical vapor deposition. *ACS Applied Materials & Interfaces* **2021,** *13* (42), 50497-50504
(21) Duanmu, Y.; Huang, Q., Analysis and optimization of the edge effect for III–V nanowire synthesis via selective area metal-organic chemical vapor deposition. *IIE Transactions* **2015,** *47* (12), 1424-1431
(22) Zhou, D.; Lang, J.; Yoo, N.; Unocic, R. R.; Wu, Q.; Li, B., Fluid-guided CVD growth for large-scale monolayer two-dimensional materials. *ACS applied materials & interfaces* **2020,** *12* (23), 26342-26349
(23) Cong, C.; Shang, J.; Wu, X.; Cao, B.; Peimyoo, N.; Qiu, C.; Sun, L.; Yu, T., Synthesis and optical properties of large-area single-crystalline 2D semiconductor WS2 monolayer from chemical vapor deposition. *Adv. Opt. Mater* **2014,** *2* (2), 131-136
(24) Andrzejewski, D.; Myja, H.; Heuken, M.; Grundmann, A.; Kalisch, H.; Vescan, A.; Kümmell, T.; Bacher, G., Scalable large-area p–i–n light-emitting diodes based on WS2 monolayers grown via MOCVD. *ACS Photonics* **2019,** *6* (8), 1832-1839
(25) Rosenberger, M. R.; Chuang, H.-J.; McCreary, K. M.; Li, C. H.; Jonker, B. T., Electrical characterization of discrete defects and impact of defect density on photoluminescence in monolayer WS2. *ACS nano* **2018,** *12* (2), 1793-1800
(26) Prasad, R. K.; Kumari, M.; Singh, D. K., Controlled Nucleation Sites with Large Coverage Area for Continuous Monolayered $WS_2$ Growth by Using the CVD Process. *Crystal Growth & Design* **2023,** *23* (11), 7744-7753

For Table of Contents Use Only

Simulation-Assisted Investigation of Curtain Gas Influence on MOCVD Growth

Feng Zhang, Fanyu Zeng, Daichi Kozawa, and Ryo Kitaura

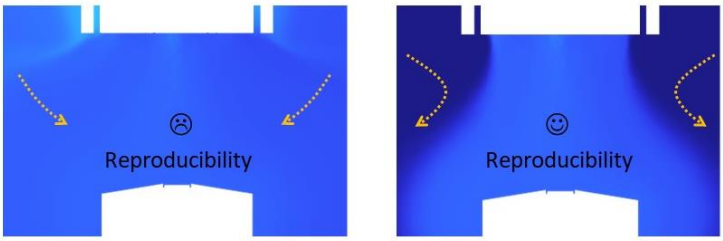


The implementation of curtain flow improves the reproducibility of MOCVD growth by creating a concentrated fluid flow around the substrate and lowering potential contamination from chamber walls.